26th EUROPEAN ROTORCRAFT FORUM

The Hague, Netherlands - 26th-29th September 2000

Paper 43

Simulation of HHC on Helicopter Rotor BVI Noise Emission using a Prescribed Wake Method

Berend G. van der Wall
DLR Institute of Flight Research, Germany

Since the HART test it is known that the changes in blade-vortex interaction locations due to HHC are caused by different tip vortex flight paths. In the past, this effect and thus the correct prediction of BVI noise could only be computed by free-wake codes. Prescribed wake codes define the tip vortex geometry in space by means of steady rotor operating parameters which are unaffected by HHC, and thus the classical prescribed wake geometry remains unchanged in HHC conditions, leading to wrong acoustic results. In this paper, a method is presented to approximately compute the influence of active rotor control on the wake geometry in the rotor disk. Using combined momentum and blade element theory, a model for the wake perturbations due to induced velocities caused by HHC is derived. The results are validated by HART data and it is proven, that the influence of HHC on vortex geometry and therewith the noise emission characteristics can be predicted sufficiently well using this methodology. The time consuming procedure of computing the wake geometry by free-wake analysis may be omitted for parameter variation studies since the wake geometry can be predicted approximately in advance.

Nomenclature

Abbreviations

AFDD	Aero Flight Dynamics Directorate
BL	Baseline case
BVI	Blade Vortex Interaction
DNW	German-Dutch Wind tunnel
HART	HHC Aeroacoustic Rotor Test
HHC	Higher Harmonic Control
IBC	Individual Blade Control
LDV	Laser Doppler Velocimetry
LLS	Laser Light Sheet
MN	Minimum Noise case
MV	Minimum Vibration case
NASA	National Aeronautics and Space Administration
ONERA	Office National D'Etudes et de Recherches Aerospatiales
PGM	Projected Grid Method
TART	Target Attitude in Real Time

Symbols

a_∞	speed of sound, m/s
A	contracted radius of downwash, hover
c	chord, m
$C(k)$	lift transfer function
C_j	coefficients of HHC-downwash
$C_{l\alpha}$	lift curve slope
C_n	normal force coeff., $= N'/(0.5\rho V^2 cR)$
C_T	thrust coefficient, $= T/(\rho\pi\Omega^2 R^4)$
f_n	radial shape function of downwash
F_j	shape function of HHC-downwash
h	vortex flight path function (basic wake)
H	vortex flight path function (HHC)
k	reduced frequency, $= \omega c/(2V)$
M	Mach number, $= V/a_\infty$
M_H	tip Mach number, $= \Omega R/a_\infty$
N'/R	local aerodynamic normal force, N/m
N_b	number of blades
r	radial coordinate, normalized by R
R	rotor radius, m
t	time, s
T	thrust, N
u, v, w	velocity components, m/s
V	velocity, m/s
x, y, z	coordinates, normalized by R
α	angle of attack, rad
β_0	blade cone angle, rad
γ	flight path angle, rad
θ	pitch angle, rad
λ	rotor inflow ratio, $= \lambda_i - \mu\tan\alpha_{TPP}$
λ_i	induced inflow ratio, $= v_i/(\Omega R)$
λ_{i0}	mean inflow ratio, $= v_{i0}/(\Omega R)$
λ_1	wake contraction rate in hover

μ	advance ratio, $= V \cos \alpha_{TPP}/(\Omega R)$
ν	natural frequency ratio, $= \omega/\Omega$
ρ	air density, kg/m^3
ϕ	vortex age in azimuth, rad
ψ	azimuth, $= \Omega t$, rad
ω	natural frequency, rad/s
Ω	rotor rotational frequncy, rad/s
Indices	
B	Beddoes
D	Drees
eq	equivalent
G	Glauert
H	hover
HHC	due to HHC
i	induced
I	inner location
n	n-th harmonic, n-th order
S	shaft
t	blade tip
tv	tip vortex
T	thrust
TPP	Tip Path Plane
0	origin, begin, mean value
Operators	
Δ	difference
$x' = dx/dr$	differentiation w.r.t. r
$\dot{x} = dx/dt$	differentiation w.r.t. time t

1 Introduction

The correct computation of the velocity field at the helicopter rotor blade during its rotation is essential to the prediction of its noise emission as well as to rotor performance and blade loads [1]. Especially the noise emission is an increasingly important criterion for helicopter certification [2]. In descent flight multiple BVI occurs on both the advancing and retreating side. A very powerful means to reduce this BVI noise is the application of HHC to the helicopter rotor, that also has shown to significantly reduce vibrations [3, 4]. The HART test, performed by DLR, AFDD, NASA, ONERA and DNW in 1994 [5, 6, 7], has brought deep inside into the physics of noise reduction: in minimum noise HHC conditions the parallel BVI on the advancing and on the retreating side can be avoided due to a very different tip vortex flight path within the rotor disk.

Within the prediction team of the HART test, each organization performed rotor simulations to compute the effects of HHC on vibration and noise. As a result it was commonly agreed that only free-wake analysis is capable of predicting the HHC effects correctly because it includes the effects of different vorticiy distributions on the wake geometry [8, 9, 10]. Prescribed wake codes are based only on steady rotor data and thus do not include the wake deformations due to HHC [11]-[16]. As an example, a classical prescribed wake [16] is used to compute the BVI mis-distance for the three HART test cases mostly referred to, namely the baseline case without HHC (BL), the HHC setting for minimum noise (MN), and that for minimum vibration (MV).

The results are given in Fig. 1 and compared to the leading edge pressure time histories of the test, which indicate well the locations of close blade-vortex interactions in the rotor disk. It can be seen, that the baseline case is matched pretty well by the prescribed wake, and that the HHC conditions are computed very similar to the baseline case with respect to BVI locations of small mis-distance. In contrast, the experiment shows significant differences between these cases due to very different vortex convection behaviour, when HHC is applied. As a result, the noise computation gives a behaviour contrary to the test: the min. noise HHC setting leads to an increse of noise while the min. vibration case leads to a slight noise reduction. Thus, classical prescribed wake is not appropriate to simulate HHC conditions with respect to noise emission, since the locations of BVI are completely missed although the different rotor loadings due to HHC are reflected in the creation of double vortex systems, where HHC caused negative loading at the blade tip.

On the other hand, free-wake analysis is a time consuming method, and thus cannot be applied for parameter variations in a wide range - this being the strength of prescribed wake methods. The subject of this paper is to fill this gap by including HHC effects into prescribed wake methods, such that HHC or IBC can be introduced into parameter studies without the penalty of increased computational effort.

2 Wind tunnel data base

The HART test and its results have been published so often, that no details are presented here again and the reader may have a look into the cited literature instead, [5, 6, 7] and [17] - [31]. Rotor data are given in Tab. 1, and all test data presented hereafter are only necessary for physical understanding of the effects and for the derivation of an additional downwash contribution due to HHC. The underlying test condition is a 6^o descent flight at moderate speed, a typical noise certification condition with maximum BVI noise emission, see Tab. 1. Three cases are of main interest: the baseline case without HHC application (BL, $\theta_3 = 0^o$), and two $3/rev$ HHC settings with different phase: the minimum vibration case (MV) and the minimum noise case (MN). The

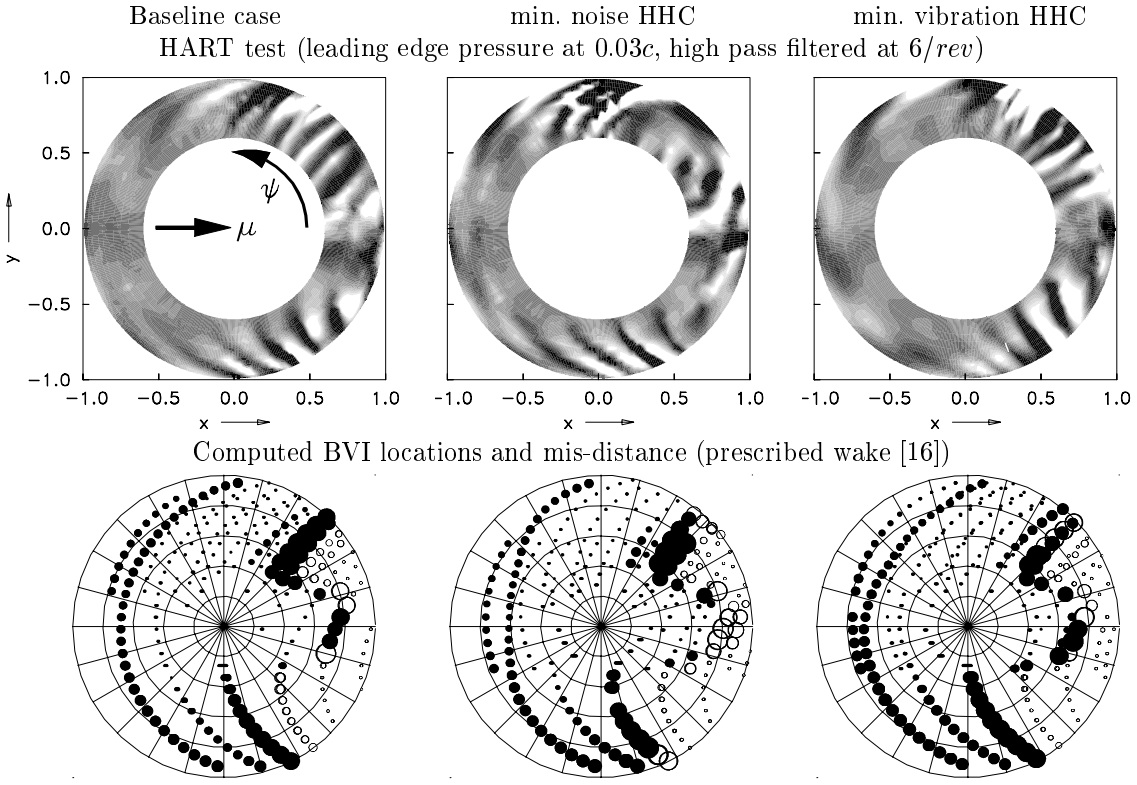

Figure 1: Comparison of BVI trajectories in the rotor disk from experiment with computed BVI mis-distance of prescribed wake. Condition of Tab. 1. Closed symbols: vortex above the blade, open: below. The symbol size indicates the closeness to the blade.

rotor data					trim condition					HHC		
c	R	r_I	θ_{tw}	β_0	M_H	γ	μ	α_S	C_T	θ_3	$\psi_{3,MN}$	$\psi_{3,MV}$
$.121m$	$2m$	.22	-8^o	2.5^o	.641	-6^o	.15	5.3^o	.0044	$.86^o$	300^o	180^o

Table 1: Rotor data, trim condition and HHC parameters, airfoil: NACA23012 mod.

HART data basis comprises the entire phase variation of ψ_n for HHC with $n = 3$, 4, and $5/rev$. In this paper, it is focused only on the $3/rev$ HHC effects, and the HHC phases of cases MN and MV are also given in Tab. 1.

The blade motion, derived from strain gauge measurements (and verified independently at several azimuthal positions by PGM and TART [5]) for flap and torsion displacements at the blade tip is given in Fig. 2. In the MN case, the vortex creation is about $2cm/1cm$ (advancing side at $\psi = 143^o$/retreating side at $\psi = 225^o$) lower than in case BL, and $1cm/1cm$ higher at the azimuth of critical BVI (advancing side at $\psi = 50^o$/retreating side at $\psi = 300^o$). Thus the BVI mis-distance is increased by $3cm/2cm$. The core diameter of the interacting vortices was measured by LDV to be in the range of $d_c \approx 0.4c \approx 5cm$. Therefore, the increased mis-distance due to blade motion alone cannot be the main source of noise reduction, especially in the view of increased vortex strength: the elastic torsion indicates $1.8^o/1^o$ larger angle of attack at the vortex generation. In the MV case, the blade tip is located $1.6cm/0.8cm$ higher than the BL case at vortex creation (with a torsion of $-2.5^o/1.1^o$), and $1cm/1cm$ lower at the position of BVI. Therefore, the vortex on the advancing side will have opposite sense of rotation, with an additional vortex inboard of conventional rotation (both have been measured by LDV).

LLS technique was used to measure blade and vortex positions shortly before the interaction takes place [32]. The result for the BVI mis-distance at the advancing side of MN case is a vortex position about $11cm$ lower than the BL case - much more than resulting from pure blade motion. Thus, the main source of noise reduction by HHC is a significantly different vortex flight path from its point of creation to that of interaction. This flight path must be a consequence of a different induced downwash field that the vortex has to pass on its way downstream. At the advancing side of the MV case, one vortex (from the blade tip) is about $17cm$ higher, and the other vortex (from inboard) is about $5cm$ higher. The

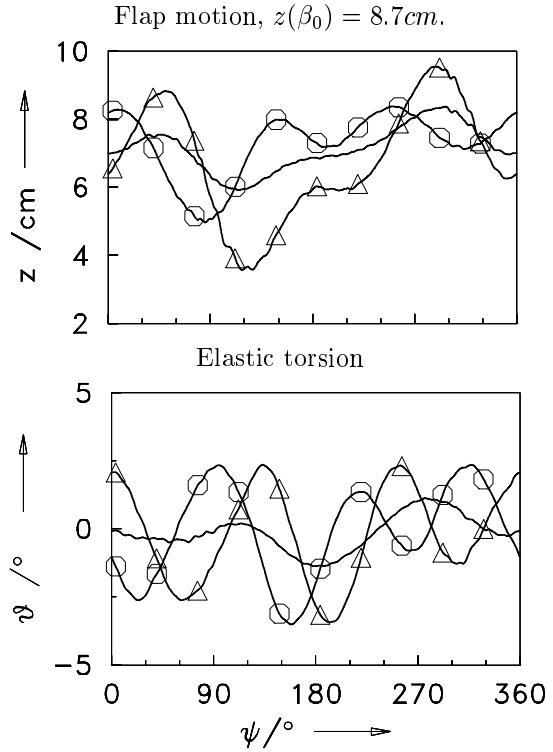

Figure 2: Blade tip motion with and without $3/rev$ HHC. BL (−), MN (△), MV (◯). Condition of Tab. 1.

LDV analysis also gives vortex positions at the advancing side [33, 34]. In MN case the vortex is found to be at least $15cm$ lower than in the BL case, and for the case MV the upper vortex (from the tip) is $9cm$ higher, the lower vortex (from inboard) $3cm$ lower than case BL. Although the absolute values obtained by LDV and LLS differ, the tendencies of both methods are the same.

Since the global thrust remains almost unchanged with and without HHC, the local thrust distribution must be the origin for different vortex flight paths. An analysis of integrated pressure distribution at sections $r = 0.75$, 0.87, and 0.97 is given in Fig. 3 in terms of the blade bound circulation, $\Gamma_b = C_n V c/2$, for the cases of interest. Herein the effects of HHC and the resulting blade torsion can be found again (compare to Fig. 2): in MN the loading is increased at the vortex creation ($\psi = 143^o$ and 225^o), therefore increasing the vortex strength. During the vortex flight path from creation through the disk to the BVI location, the vortex has to pass a higher loading on both sides compared to case BL. This explaines the significantly increased BVI mis-distances at the BVI locations ($\psi = 50^o$ and 300^o). In the MV case, the advancing side exhibits strong negative loading at the vortex creation ($\psi = 143^o$), thus the tip vortex has opposite sense of rotation and gets blown upwards on its way downstream. The inboard vortex of conventional rotation does not pass this upwash area and thus stays lower.

From elastic torsion and the measured lift in terms of $C_n M^2$, a transfer function can be identified that relates the HHC input at frequency n, θ_n, to the resulting pitch angle at a given radial station. The elastic torsion and the natural frequency in torsion do play a major role in amplification and phase shift. This is especially true for the relatively soft-in-torsion Bo105 rotor ($\nu_\vartheta = 3.7$), used as model within the HART test. Obviously, a $3/rev$ HHC will get a significant amplification (see Fig. 2), while a control with $n > 3$ will get a significant phase shift with a reduction of amplitude. Then, the angle of attack due to pitch oscillations can be computed. The remaining transfer function from this angle of attack to the measured lift may be viewed as a sort of unsteady lift transfer function, representing the inflow contributions, and at $r > 0.9$ this also includes the three-dimensional flow around the tip. It is important to keep in mind that in forward flight a single frequency input in the control angle results in a broader spectrum of lift harmonics around the control frequency. Thus, an n/rev HHC input results in a lift output from basically $n \pm m/rev$ with $m = 2$.

To create such transfer functions, at each i/rev (with $n-m \le i \le n+m$) the local angle of attack derived from pitch has to be analysed for all the HHC variations and the case BL. The difference from BL to the HHC condition at each frequency provides the transfer function from HHC input to angle of attack output, $\Delta\alpha_i/\Delta\theta_n$. The mean influence is found at $i = n$, and all side harmonics may be referenced to this ratio.

$$\frac{\Delta\alpha}{\Delta\theta_n} = \left|\frac{\Delta\alpha_n}{\Delta\theta_n}\right| \sum_{i=n-m}^{n+m} \left|\frac{\Delta\alpha_i}{\Delta\alpha_n}\right| \cos(i\psi - \psi_n - \Delta\psi_{in}) \tag{1}$$

Two side harmonics ($m = 2$) cover the interesting range of influence on angle of attack. The result for $3/rev$ HHC, derived from HART data, is given in Tab. 2. The same can be done for the lift transfer function, given also in Tab. 2, where the difference in $C_n M^2$ from BL to HHC is related to the HHC input. It can be seen, that the lift has a phase lag relative to the angle of attack at the control frequency. Finally, the lift of each harmonic can be referred to the appropriate angle of attack, leading to a lift deficiency function. With the local reduced frequency $k = k_t/r$ and $k_t = c/(2R)$, this function is defined as $C(k) = \Delta C_n M^2/(2\pi r^2 M_H^2 \Delta\alpha)$ with a phase shift of $\psi_{C(k)} = \psi_{in}(C_n M^2) - \psi_{in}(\alpha)$. The result is given in Tab. 3. At constant frequency of $3/rev$ the phase lag increases inversely to the radial position, an effect to be explained by the reduced

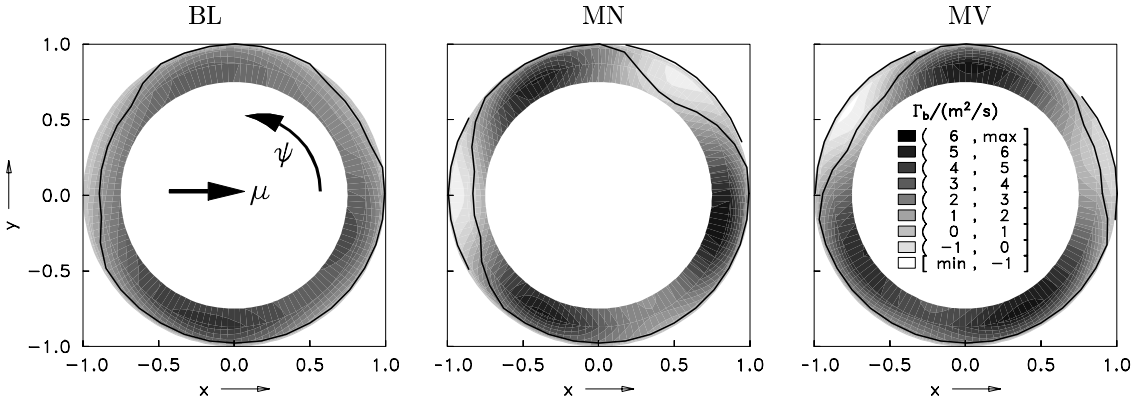

Figure 3: Blade circulation distribution and derived vortex creation locations. Condition of Tab. 1.

r	$\left\lvert\frac{\Delta\alpha_i}{\Delta\alpha_n}\right\rvert$ at $i=$			$\Delta\psi_{in}/^o$ at $i=$			$\left\lvert\frac{\Delta C_n M^2\lvert_i}{\Delta C_n M^2\rvert_n}\right\rvert$ at $i=$			$\Delta\psi_{in}/^o$ at $i=$		
	$n-2$	$n-1$	$n+1$	$n-2$	$n-1$	$n+1$	$n-2$	$n-1$	$n+1$	$n-2$	$n-1$	$n+1$
.75	.07	.23	.21	116	348	329	.08	.57	.17	12	359	233
.87	.09	.26	.19	122	340	328	.12	.49	.18	58	344	218
.97	.10	.29	.18	125	335	327	.14	.47	.16	80	333	209

Table 2: Spectra of side harmonics of blade section angle of attack and lift at $3/rev$ HHC. The amplitudes are referenced to the appropriate $3/rev$ response.

r	.75	.87	.97
$\left\lvert\frac{\Delta\alpha_n}{\Delta\theta_n}\right\rvert$	2.39	2.45	2.48
$\Delta\psi_n/^o$	54	48	43
$\left\lvert\frac{\Delta C_n M^2\lvert_n}{\Delta\theta_n}\right\rvert$	2.68	3.99	3.02
$\Delta\psi_n/^o$	61	56	47
$\left\lvert\frac{\Delta C_n M^2}{\Delta\alpha}\right\rvert$	1.12	1.63	1.22
k	.121	.105	.094
$\lvert C(k)\rvert$	.77	.83	.51
$\psi_{C(k)}/^o$	7	8	4

Table 3: Transfer functions at $n=3/rev$ HHC.

frequency that also increases due to its proportionality to $1/r$. The magnitude of the lift deficiency function decreases with increasing reduced frequency, and at the tip the three-dimensionality of the flow additionally reduces $C(k)$.

3 Prescribed wake models

Prescribed wake codes can be traced back to 1956, where for hover condition a parametric model was build up, based on flow visualization of wind tunnel experiments [11]. The widely known model of Landgrebe is dated to 1971 for hover and includes rotor loading, number of blades and twist in its parametric description [12, 13]. In forward flight, the UTRC Generalized Wake is widely used [15]. Its parameters are also based on wind tunnel tests and the wake geometry depends basically on C_T and μ. The latest prescribed wake variant stems from Beddoes and was published in 1985 [16]. Again, the wake geometry is based on steady rotor operational data, and the roll-up at the left and right of the disk is empirically formulated.

Several downwash models exist that are describing the induced velocity distribution within the rotor disk instead of the locations of tip vortices. These are typically derived from momentum theory or actuator disk assumptions, like Glauerts downwash [35] (that is basis of Beddoes geometry), additional lateral asymmetries in forward flight given by Drees [36], or the model of Mangler [37, 38, 39]. A prescribed wake geometry can always be computed using one of these downwash models, and it is somewhat surprising that Manglers model has never been used as a basis for such a wake (although it computes local mean induced velocities sufficiently well).

For computation of the vortex wake geometry at every instance of time, the mean induced velocity distributions must be known analytically in advance. For this purpose, momentum theory (like Glauerts downwash, that forms the basis of Beddoes wake geometry) or actuator disk theory (like Manglers downwash) can be used. The essential problem is that the downwash models are build up in polar coordinates that are advantageous for rotor simulation purposes, but disadvantageous for vortex flight path integration, since the polar coordinates have to be transformed into cartesian coordinates first. As long as the radial distribution is of low order in r and

only one harmonic is used (like in Glauerts downwash: $\lambda_{iG}/\lambda_{i0} = k_0 + k_x r\cos\psi$ with $k_0 = 1$), the transformation leads to terms proportional to x and the integration is simple.

$$\frac{\lambda_{iG}}{\lambda_{i0}} = k_0 + k_x x = f_G \tag{2}$$

Therein the gradient $k_x = |\arctan(\mu/-\lambda)|$ is due to forward flight. Additional lateral asymmetries are formulated by Drees through $\lambda_i/\lambda_{i0} = -2\mu y = f_D$ and may simply be added. The transformation of Manglers downwash, however, leads to very complicated expressions to be integrated. This might have been a reason not to use this downwash model in the past. A general formulation of downwash geometries will always be defined as a Fourier series like

$$\frac{\lambda_i}{\lambda_{i0}} = \sum_{n=0}^{\infty} c_n f_n(r) g_n(\psi) \tag{3}$$

where λ_{i0} results from momentum theory in forward flight and is depending on α_{TPP}, μ and C_T. f_n are radial shape functions of higher order in r. With the help of Moivre's formula the trigonometric functions g_n of argument $n\psi$ can be transformed to those with argument ψ only, but to the power of n [40].

$$\begin{aligned}\cos n\psi = \cos^n\psi \quad & - \binom{n}{2}\cos^{n-2}\psi\sin^2\psi \\ & + \binom{n}{4}\cos^{n-4}\psi\sin^4\psi \\ & - \cdots + \cdots\end{aligned} \tag{4}$$

A similar expression exists for $\sin n\psi$. Next, $\cos\psi = x/r$, $\sin\psi = y/r$, $r^2 = x^2 + y^2$ have to be introduced in order to obtain the induced velocity field in terms of x and y only. This is necessary before integrating the vortex flight path along the x coordinate through the downwash field, assuming no variation in vertical direction. Strictly speaking, this is a crude assumption (especially above the disk), but the vortices do move with the wake and thus always remain in close vicinity of the dwonwash field.

Beddoes downwash superimposes a lateral distribution proportional to y^3:

$$\frac{\lambda_{iB}}{\lambda_{i0}} = f_G + f_B \qquad f_B = \frac{8}{15\pi} - k_x|y^3| \tag{5}$$

The factor $8/(15\pi)$ was not given by Beddoes in [16], but omitting it would violate the momentum theory result for the mean value and thus lead to erraneous wake geometries. For the wake geometry it also is important that the lifting part of the blade does not extend from the rotor center to the full span as assumed by momentum or actuator disk theory. A real blade's lift essentially

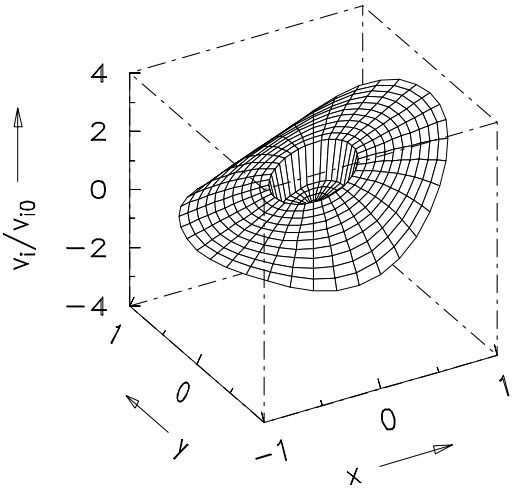

Figure 4: Downwash distribution of the modified prescribed wake, condition of Tab. 1.

is provided between approximately $r = 0.3$ and about $r = 0.96$. Then, in order to fulfil the total momentum on a reduced lifting area of the disk, the mean value of induced velocities must be multiplied by 1.2 in case of Glauert's downwash.

$$1 \stackrel{!}{=} 2k_0\bar{k}_0\int_{0.3}^{0.96} r\,dr \qquad \Rightarrow \qquad \bar{k}_0 = 1.2 \tag{6}$$

This correction is smaller for the Mangler downwash (1.07, see [46]) since the shape function f_0 has already small values in the center of the disk, while Glauerts distribution is constant everywhere ($k_0 = 1$). By doing so, all vortex elements passing the center of the disk are not affected by the mean induced velocity as long as they are within $r < 0.3$, and thus are at a higher flight path in the rear of the disk. This has been also observed in wind tunnel tests as well as in free-wake computations. As a result of these modifications, the downwash distribution of the modified model is given in Fig. 4.

The vortex flight path can now be obtained by integration over the nondimensional time Φ until its instantaneous age ϕ. It is easier to transform in and integrate along $x = r\cos\psi = \mu\phi + x_0$ instead, where $d\Phi = dx/\mu$ and the creation of the vortex element is $x_0 = r_{tv}\cos\psi_v$ at a lateral position of $y_0 = r_{tv}\sin\psi_v$. Note that r_{tv} not necessarily is at the blade tip, see Fig. 3. The integration results in nondimensional vortex flight path functions.

$$\int_0^{\phi} f_n g_n\,d\Phi = \frac{1}{\mu}\int_{x_0}^{x} f_n g_n\,dx = \frac{h_n}{\mu} \tag{7}$$

For the derivation of these complex expressions h_n, (for Mangler's downwash they are given in [46]), a software capable of symbolic algebra was used [41]. Then, the vertical coordinate along the

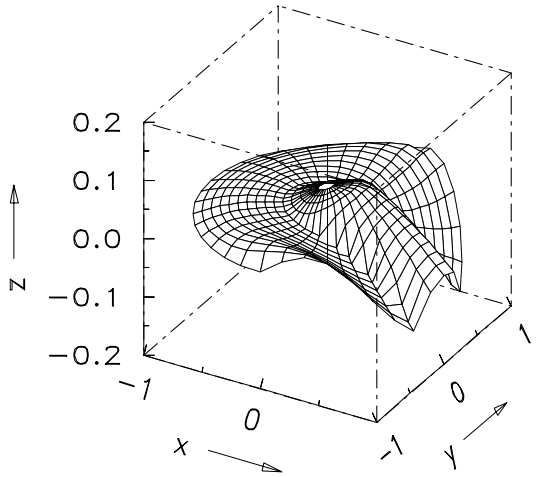

Figure 5: Tip vortex flight path using modified prescribed wake, condition of Tab. 1.

tip vortex flight path using a general downwash as basis is given by

$$z = \int_0^{\phi} -\lambda_i \, d\Phi = -\frac{\lambda_{i0}}{\mu} \sum_{n=0}^{\infty} c_n h_n \qquad (8)$$

The functions h_n will become very complex and lengthy with increasing n. Since the downwash contribution of the higher orders of n is typically of decreasing nature within the disk and mainly contributes to the convergence at the blade tip itself, terms above $n = 6$ are mostly negligible. Now the vortex flight path using Beddoes model, based on the modified Glauert downwash (two terms are present: $n = 0, 1$) and the lateral contribution due to Drees, can be computed.

$$z_B = -\frac{\lambda_{i0}}{\mu} \int_{x_0}^{x} f_G + f_B \, dx = -\frac{\lambda_{i0}}{\mu} h_B \qquad (9)$$

with the flight path function

$$\begin{aligned} h_B &= \int_{x_0}^{x} \frac{8}{15\pi} - k_x|y^3| - 2\mu y + k_0 + k_x x \, dx \\ &= \left[\left(\tfrac{8}{15\pi} - k_x|y^3| - 2\mu y + k_0 \right) x + \tfrac{k_x}{2} x^2 \right]_{x_0}^{x} \end{aligned} \qquad (10)$$

Care must be taken to the inner part of the disk with no contribution from the mean induced velocity. Here, a stepwise integration has to be applied. The rest of the wake geometry strictly follows Beddoes approach and is not repeated here. For a typical descent flight condition, the resulting tip vortex flight path surface using this modified Beddoes downwash is presented in Fig. 5. It can be seen that in the rear part with $|y| < 0.4$ the vortices are located higher due to the effect of root cutout on the mean induced velocity.

In hover, the division by μ leads to a singularity and the functions h_n are not valid there. This is because the functions f_n are no longer depending on ϕ, and the integration is much simpler as in forward flight: $z = -\lambda_{i0} c_0 f_0 \phi$. Also, in a general model all terms with $n > 0$ will vanish, but the shape function f_0 will be any function of r like in [38]. Then the radial vortex position is a function of its age (due to contraction of the downwash stream tube) and the result is more complicated. For Mangler's downwash model, the resulting flight path function is given in [46].

4 Modelling HHC effects

In order to compute tip vortex deflections due to HHC, the contributions of HHC to the induced velocity field have to be known in advance. For this purpose, the results from Sect. 2 can be used. First, it was shown that the lift response at n/rev can be described in dependency of the resulting angle of attack (control and elastic torsion contributions) using the transfer function from pitch input to this angle of attack and that one from pitch input to the resulting lift. Elastic torsion plays an important role therein. Second, it was shown that the side frequency at $n-1/rev$ is an important part of the lift resulting from n/rev HHC.

It must be recalled that HHC is an integer multiple of the rotor rotational frequency, and thus a steady phenomenon for an observer located outside - the additional lift due to HHC appears as a wave being fixed in space, although it is an unsteady phenomenon for the rotating blade. Therefore, the HHC-induced thrust distribution is steady from an actuator disk point of view and its geometry can be expressed in form of a Fourier series. Now momentum theory can be applied for the amplitude of this Fourier series as it is used for computation of the mean induced velocity v_{i0}, which is based on the mean value of the thrust. Then, combined blade element/momentum theory may be applied using the amplitude of angle of attack to compute HHC-induced downwash. The local unsteady thrust of the blade element is

$$dT = N_b \frac{\rho}{2} (\Omega R r)^2 c C_{l\alpha} C(k) \left(\theta - \frac{v_i}{\Omega R r} \right) R \, dr \qquad (11)$$

By momentum theory this differential thrust is expressed by the mass flow $\dot{m}$ and the total increase in velocity of the slipstream, w [42, 43].

$$\begin{aligned} dT &= d\dot{m}\, w \\ &= (\rho 2\pi R^2 r \, dr \, v_i)(2v_i) \\ &= 4\rho\pi v_i^2 R^2 r \, dr \end{aligned} \qquad (12)$$

From both results a quadratic expression for v_i can be derived and from this the induced inflow

$\lambda_i = v_i/(\Omega R)$.

$$\lambda_i = \frac{N_b c C_{l\alpha} C(k)}{16\pi R}\left(\sqrt{1+\frac{32\pi R r\theta}{N_b c C_{l\alpha} C(k)}}-1\right) \tag{13}$$

In steady conditions (collective control in hover) $C(k) = 1$ and this reduces to the formula found in classical literature [42, 43]. Setting $C_{l\alpha} = 2\pi$ and $k = nk_t/r$ with $k_t = c/(2R)$ the result is

$$\lambda_i = \frac{N_b k_t C(k)}{4}\left(\sqrt{1+\frac{8r\theta}{N_b k_t C(k)}}-1\right) \tag{14}$$

In general, the induced velocity field due to HHC may be expressed in form of a Fourier series in azimuth and radial shape functions similar to Manglers downwash. Knowing that an input at n/rev also results in side harmonics (in forward flight) as shown in Sect. 2, the induced downwash will also incorporate these side harmonics.

$$\begin{aligned}\lambda_i(r,\psi) &= C_j F_j(r)\sum_n \lambda_{in}(\alpha_n) \\ &\quad\times \sum_{i=n-m}^{n+m}\frac{A_{in}}{A_n}\cos(i\psi-\psi_n-\psi_{A_{in}})\end{aligned} \tag{15}$$

To ease the analysis, the amplitudes of this downwash model are evaluated at a representative radial station, for example $r = 0.75$ or 0.87. The radial distribution is advantageous from an analytical point of view, when it is expressed by $F_j(r) = r^j$ with orders $j = 0$, 1, or 2, representing a constant distribution over span, a linear increasing distribution, or proportional to r^2, respectively. The highest order seems plausible with respect to the quadratic increase of lift to the tip, while lower orders are simpler to integrate later on. The factor C_j takes care for the total momentum that must be retained for any of the distribution functions F_j. Thus,

$$1 \stackrel{!}{=} 2C_j\int_{r_I}^1 F_j(r) r\,dr \qquad \rightarrow C_j = \frac{j+2}{2(1-r_I^{j+2})} \tag{16}$$

The amplitude of HHC induced downwash λ_{in} depends on the amplitude of dynamic lift, the lift depends on the actual amplitude of angle of attack, and this is widely depending on elastic torsion properties of the blade as shown before. In addition unsteady aerodynamic phenomena are in effect. All these effects can now be introduced using the results of Sect. 2 and the expression for the induced velocities above at a representative radial station r_{ref}.

r	.75	.87	.97
$\lambda_{i,n}$	.0215	.0249	.0234
$\Delta\psi_{i,n}/^o$	61	56	47
$\lambda_{i,n-1}$	.0123	.0122	.011
$\Delta\psi_{i,n-1}/^o$	359	344	333

Table 4: Amplitude and phase of $n = 3/rev$ HHC induced downwash at the control frequency and the most important side frequency. Condition see Tab. 1, $\theta_3 = 1^o$, $\psi_3 = 0^o$.

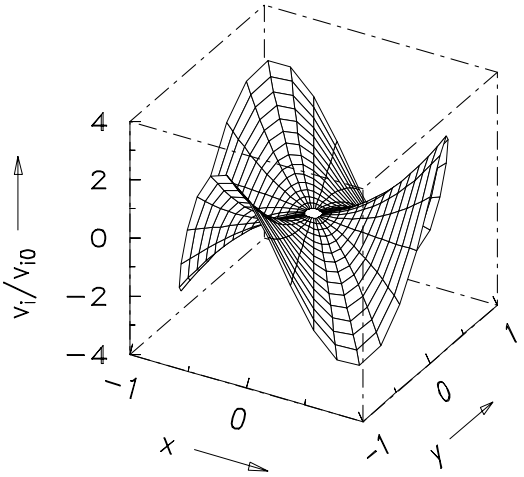

Figure 6: Induced downwash due to $3/rev$ HHC. $\mu = 0.15$, $\theta_3 = 1^o$, $\psi_3 = 0^o$, $j = 2$.

$$\lambda_{in}(r_{ref}) = \frac{N_b k_t |C(k(r_{ref})|_n}{4} \times\left(\sqrt{1+\frac{8r_{ref}\left|\frac{\Delta\alpha}{\Delta\theta_n}(r_{ref})\right|}{N_b k_t |C(k(r_{ref})|_n}\theta_n}-1\right) \tag{17}$$

For $n = 3/rev$ HHC of amplitude $\theta_3 = 1^o$ the resulting induced velocity amplitudes are computed using the transfer function data given before and the result is given in Tab. 4. For all following applications, the reference radius of $r = 0.75$ is chosen. In Fig. 6 the resulting induced velocity field due to $3/rev$ HHC is shown.

The perturbation of the tip vortex flight path within the rotor disk due to this HHC induced velocity field is obtained by analytical integration as has been shown in the last section. Using Moivre's formula [40] for transforming the higher harmonics into powers of the basic harmonic and putting in the relationships $\cos\psi = x/r$, $\sin\psi = y/r$ it is possible to integrate the vortex flight path from its origin at x_0 to any instantaneous position x.

$$\int_0^\Phi F_j g_n\,d\phi = \frac{1}{\mu}\int_{x_0}^x F_j g_n\,dx = \frac{H_{nCj}}{\mu} \tag{18}$$

These H_{nCj} are nondimensional flight path functions of the $\cos n\psi$ term with the jth order of F as radial distribution function. For $j = 2$ and $n = 2, 3$, the functions H_{nCj} and H_{nSj} are

$$\begin{aligned} H_{nCj} &= \int_{x_0}^{x} r^j \cos(n\psi)\, dx \\ H_{nSj} &= \int_{x_0}^{x} r^j \sin(n\psi)\, dx \\ 3H_{2C2} &= \left[x^3 - 3y^2 x\right]_{x_0}^{x} \\ H_{2S2} &= y\left[x^2\right]_{x_0}^{x} \\ 3H_{3C2} &= \left[(x^2 - 11y^2)\sqrt{x^2+y^2}\right]_{x_0}^{x} \\ 2H_{3S2} &= 3y\left[x\sqrt{x^2+y^2}\right]_{x_0}^{x} \\ &\quad -5y^3\left[\log\left(x+\sqrt{x^2+y^2}\right)\right]_{x_0}^{x} \end{aligned} \tag{19}$$

For $j = 0$, 1, 2 and $n = 1$ to 6 and for the hovering case where $\mu = 0$, the results are given in [46]. Due to the complexity, again symbolic algebra software is used for deriving these functions [41]. Finally, the total flight path at multiple n/rev HHC is computed by

$$\begin{aligned} z_{HHC} &= -\frac{C_j}{\mu}\sum_n \lambda_{in} \sum_{i=n-m}^{n+m} \frac{A_{in}}{A_n} \\ &\quad \times[\cos(\psi_n + \psi_{A_{in}})H_{nCj} \\ &\quad + \sin(\psi_n + \psi_{A_{in}})H_{nSj}] \end{aligned} \tag{20}$$

For the case MN of the HART test ($\theta_3 = 0.86^o$, $\psi_3 = 300^o$) and MV ($\theta_3 = 0.86^o$, $\psi_3 = 180^o$) the resulting tip vortex flight path surfaces only due to HHC have been computed and they are plotted in Fig. 7. They are to be seen as additional deflections to be superimposed on any basic model of prescribed wake, thus they are the difference to the BL case. The viewpoint is left behind the disk such that the differences on the advancing side are best visible. For this plot, the tip vortex is assumed to be created at the tip of the rotor. In the MN case, $y > 0.4$, the vortex flight path is significantly below zero ($z_{HHC} = -0.1$). On the retreating side the flight path also is below zero. Thus, the BVI mis-distance is largely increased and a reduced BVI noise emission will be the result. In the center ($-0.1 < y < 0.4$) the entire flight path is pushed upwards by HHC.

The case MV lifts the tip vortex flight path on the advancing side to some degree such that BVI will occur more downstream compared to the BL case. This is due to the effect of download in the second quadrant (see Fig. 3) inducing an upwash, that blows up the tip vortex on its way downstream. A vortex created more inboard as is true for the MV case does not have to pass this upwash area, because it is created downstream of it and thus will create BVI as in the BL case. The increased blade lift around $\psi = 180^o$ leads to an increased downwash in the center area $-0.5 < y < 0.2$, pushing the tip vortices downwards.

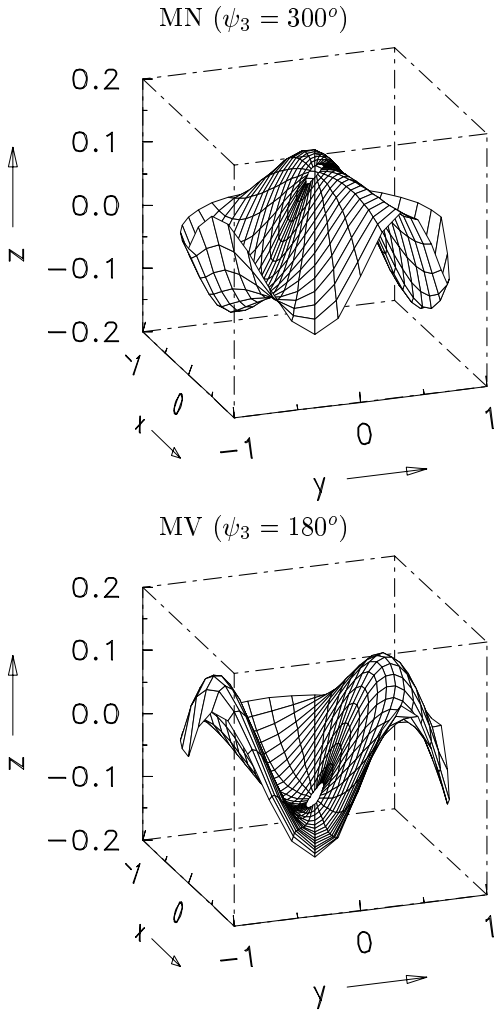

Figure 7: Tip vortex flight path surface due to $3/rev$ HHC with $\theta_3 = 0.86^o$. The side harmonic $n - 1 = 2/rev$ is included. Condition of Tab. 1, $j = 2$.

5 Validation of the method

First, the BL case will be considered. In Fig. 8 the resulting trajectories of BVI within the disk are compared. Test data are available in form of high pass filtered pressure distribution of the leading edge sensors that reflect well the location and intensity of BVI. In computation, the intensity is expressed via closeness of predicted tip vortices to passing blades: the smaller the BVI mis-distance, the larger the symbol. Open symbols denote vortices below the disk and closed symbols those being above.

Results for MN and MV cases are also presented in Fig. 8 and Fig. 8. In the MN case, there is no BVI present in the first quadrant at the blades tip - this being the reason for reduced noise emission. The vortices are passing the blade far enough below it not to create high frequency loading. The interactions have moved to $y = 0.5$ and

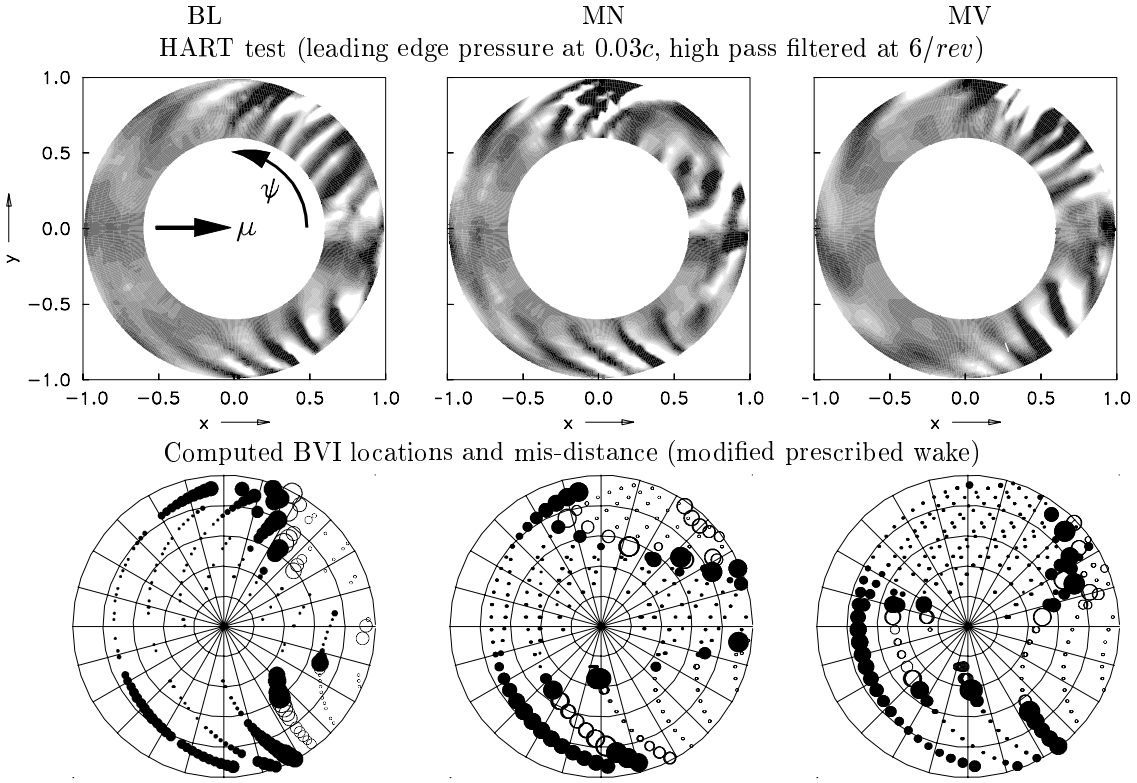

Figure 8: Comparison of BVI trajectories in the rotor disk from experiment with computed BVI mis-distance of prescribed wake. Condition of Tab. 1. Closed sybols: vortex above the blade, open: below. The symbol size indicates the closeness to the blade.

to $\psi = 90^o$ instead, where they are less important with respect to noise. The retreating side shows similar behaviour since the strong parallel interaction at $\psi = 300^o$ now is less important, the vortex is below the blade. Both effects are due to increased lift in the second and third quadrant (see Fig. 3), leading to increased downwash at these areas, and thus the tip vortices are "blown down" on their way through the disk. The MV case exhibits opposite trends. Here, the most severe interactions have moved right to the blade tip in the first quadrant, where the highest local Mach numbers are present and thus BVI generates more noise compared to the BL case. Also, the retreating side shows the strongest interaction right at the location of parallel BVI at $\psi = 300^o$.

At $y = 0.6$ LDV measurements have been performed during HART. From these data the position of the vortex center can be analysed when passing the LDV location. A comparison of the computed vortex flight path within this lateral plane can then be used for validation. This is done in Fig. 9 for case BL with the modified Beddoes model. The wind tunnel coordinate system is used and the blades are plotted as straight lines from the origin at the hub. The vortex passage is predicted rather close to the measured location (+). It can be seen, that the vortices are not created at the tip but at a radial position somewhat inboard. This is a result of the radial distribution of bound circulation that shows a small gradient at the tip, see Fig. 3. Results using the Mangler model are given in [46].

In Fig. 9, for cases MN and MV the resulting flight path using the modified Beddoes model and superimposed by the HHC perturbations is compared to the measured location (LDV in case MV with two vortices, LLS in case MN). It can very clearly be seen that the difference of BVI location is generated by a significant different flight path of the tip vortices. In case MV, the tip vortex (with opposite sense of rotation) as well as the inboard vortex (with conventional sense of rotation) are pushed up due to negative blade lift in the tip region, see Fig. 3. In contrast, the case MN shows the vortex passing the blade very early (at $x = -0.25$) and staying below the disk such that it is significantly below the blade where parallel BVI can occur ($x \geq 0.5$). This is caused by increased blade lift and thus increased downwash in the second quadrant, see Fig. 3. The difference in blade position due to HHC can also be seen in Fig. 9 and it is obvious that the changes in the vortex flight path are larger by about one order of magnitude. Thus, the different blade flap motion is unimportant for BVI; the major effect of noise reduction stems from the vortex flight path.

Further validation data require a rotor simula-

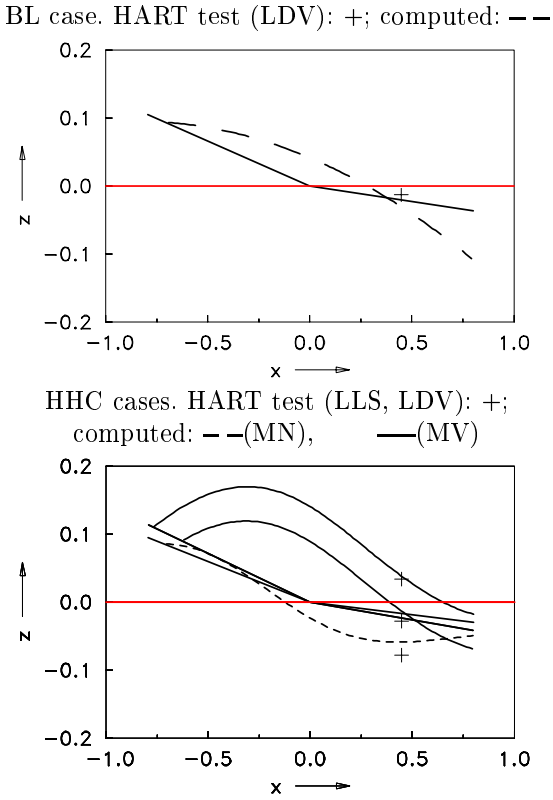

Figure 9: Computed vortex flight paths on advancing side at $y = 0.6$ for case BL, MN and MV (with double vortex system, see Fig. 3), condition of Tab. 1.

tion with elastic blades, unsteady aerodynamics and the wake described before. The code used is an isolated rotor simulation program trimming the basic controls to the desired rotor thrust and moments at given operational conditions [44]. Among other applications, this code proved to be well suited for rotor performance prediction as well as for the prediction of unsteady aerodynamic loads [45]. In Fig. 10, the elastic blade deflection in flap and torsion at the blade tip and the lift at $r = 0.75$ and $r = 0.87$ is compared to the experiment. The offset in flap motion is a result of a zero precone in the computation, while it is $\beta_0 = 2.5^o$ in the experiment, see Tab. 1. There is more flap motion in the computation than in the experiment, but the elastic torsion is met quite well. The sectional lift in form of $C_n M^2$ at the given radial stations do also match the experimental data, especially in the location and amplitudes of BVI related fluctuations. This is important for the noise computation based on sectional loading time histories.

Finally, the noise emission computed from the simulated loading distributions with and without HHC is compared to the test data, where microphones scanned the acoustic emission in a plane $1.5R$ below the rotor. Using Ffowks-Williams-Hawkins equation,[1] the loading distribution can be used as input, together with operational conditions, blade motion and geometrical rotor data, to obtain pressure time histories due to thickness and loading (except shock wave noise) at any location in space. The result for the noise levels in the same plane as where they were measured is given in Fig. 11 using the modified Beddoes model only (BL) and superimposed by the HHC wake deflections (MN and MV). It can be seen that the general trends are predicted well in terms of noise level and directivity. Without the HHC related wake deflections, the MN case would even generate more noise than the case BL (see Fig. 1), since the BVI locations remain the same (due to unchanged vortex wake geometry and unchanged BVI mis-distance), but the vortex strength at the interaction is significantly incresed by the HHC related loading, see Fig. 3. Therefore, although the method presented in this paper is only an approximate one, the HHC induced changes of tip vortex flight paths within the rotor disk are computed to an order of accuracy being enough for principle investigations.

More results for $n = 4$ and $5/rev$ HHC as well as for $2/rev$ IBC can be found in [46].

6 Conclusions

In this paper, the development and validation of a prescribed wake method to compute the tip vortex flight path under HHC/IBC conditions is described. The conclusions can be summarized as:

- Elastic blade behaviour plays an important role in amplifying or reducing the HHC input by its natural frequency in torsion.
- Using blade element and momentum theory a HHC induced downwash field can be formulated.
- In analogy to the computation of the mean induced velocities from steady rotor data like C_T, the HHC related downwash requires information about the dynamic rotor properties like natural frequency in torsion.
- The tip vortex flight path perturbation is obtained by analytical integration through the HHC induced downwash field.

The presented prescribed wake method includes HHC effects on the wake geometry and appears to be well suited for an approximate estimation of the radiated BVI noise emission in forward flight.

[1] The acoustic computation has been performed by the DLR Institute of Desing Aerodynamics using the code AKUROT

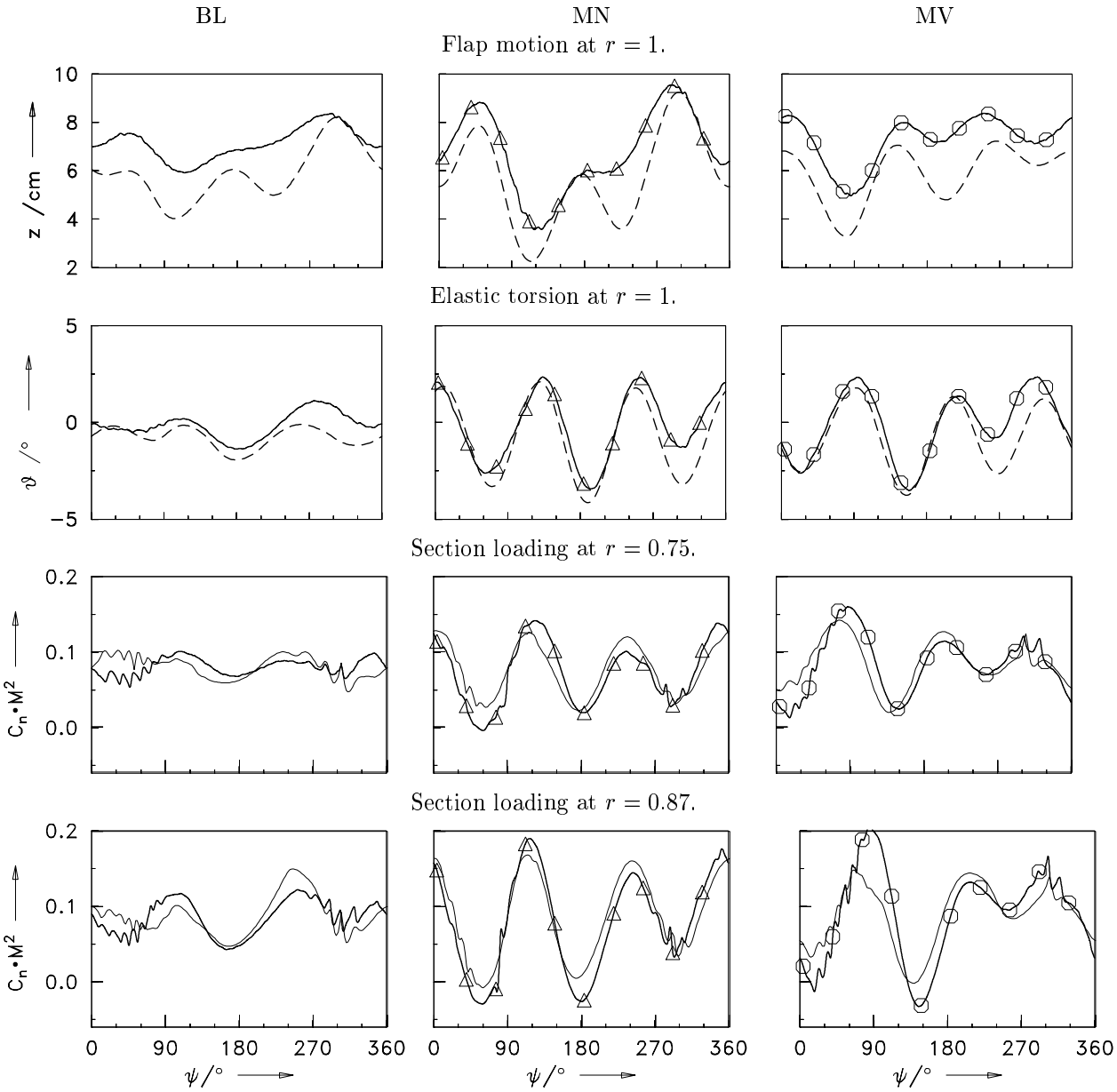

Figure 10: Comparison of computed blade deflections and sectional loading with HART data, condition of Tab. 1. Experiment: ━━, computed: – –

Results obtained for 3/rev HHC compare well to wind tunnel test data.

Although the method presented in this paper is only an approximate one, the HHC induced changes of tip vortex flight paths within the rotor disk are computed to an order of accuracy being enough for principle investigations. With this method, it is now possible to use fast prescribed wake methods for HHC and IBC investigations with respect to blade loading and acoustics of a helicopter rotor. Thus, time consuming free-wake codes are not mandatory any more for computing the acoustic emission of a rotor under HHC/IBC conditions. The method is therefore intended to be a major step forward towards numerical application of HHC and IBC.

References

[1] A.J. Landgrebe, *New Directions in Rotorcraft Computational Aerodynamics Research in the U.S.,* AGARD-CP-552, Paper 1, 1995

[2] *International Standards and Recommended Practices, Environmental Protection,* ICAO, Annex 16, Vol. 1, Aircraft Noise, USA, 1988

[3] R. Kube, *Einfluß der Blattelastizität auf die höherharmonische Steuerung und Regelung eines gelenklosen Hubschrauberrotors,* DLR FB 97-26, Germany, 1997

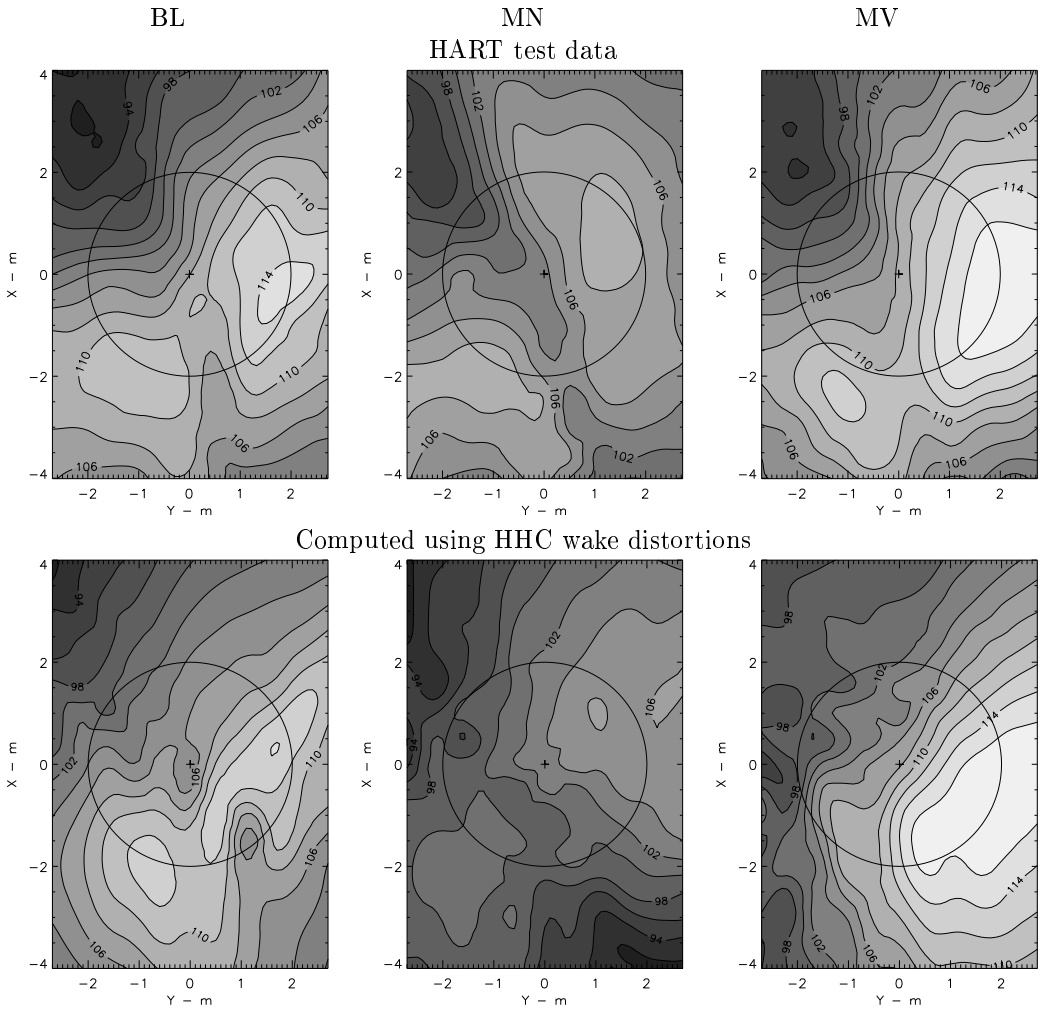

Figure 11: Comparison of mid-frequency noise level $L-MF$ from test and simulation for cases BL without HHC and with $3/rev$ HHC for cases MN and MV. Wind is from top to bottomn, x here is upstream.

[4] W.R. Splettstößer, R. Kube, U. Seelhorst, W. Wagner, A. Boutier, F. Micheli, E. Mercker, K. Pengel, *Key results from a Higher Harmonic Aeroacoustic Rotor Test (HART) in the German-Dutch Wind Tunnel,* 21^{st} European Rotorcraft Forum, Saint-Petersburg, Russia, 1995

[5] W.R. Splettstößer, R. Kube, U. Seelhorst, W. Wagner, A. Boutier, F. Micheli, *Higher Harmonic Control Aeroacoustic Rotor Test (HART) - Test Documentation and Representative Results -,* DLR IB 129-95/28, Braunschweig, Germany, 1995

[6] Y.H. Yu, B. Gmelin, H. Heller, J.J. Philippe, E. Mercker, J.S. Preisser, *HHC Aeroacoustic Rotor Test at the DNW - The Joint German/French/US HART Project -,* 20^{th} European Rotorcraft Forum, Amsterdam, Netherlands, 1994

[7] B.L. Gmelin, H.H. Heller, E. Mercker, J.J. Philippe, J.S. Preisser, Y.H. Yu, *The HART Programme, a Quadriliteral Cooperative Research Effort,* 51^{st} Annual Forum of the American Helicopter Society, Ft. Worth, TX, USA, 1995

[8] T.F. Brooks, D.D. Boyd, Jr., C.L. Burley, J.R. Jolly, Jr., *Aeroacoustic Codes For Rotor Harmonic and BVI Noise - CAMRAD.Mod1/HIRES,* 2^{nd} AIAA/CEAS Aeroacoustics Conference, State College, PA, USA, 1996

[9] B. Michea, A. Desopper, M. Costes, *Aerodynamic Rotor Loads Prediction Method with Free Wake for Low Speed Descent Flight,* 18^{th} European Rotorcraft Forum, Avignon, France, 1992

[10] B.G. van der Wall, M. Roth, *Free-Wake Analysis on Massively Parallel Computers and Validation with HART Test Data,* 53^{rd} Annual Forum of the American Helicopter Society, Virginia Beach, VA, USA, 1997

[11] R.B. Gray, *An aerodynamic Analysis of a Single-Bladed Rotor in Hovering and Low Speed Forward Flight as Determined from the Smoke Studies of the Vorticity Distribution in the Wake,* Princeton Aeronautical Engineering Department Report No. 356, USA, 1956

[12] A.J. Landgrebe, *An Analytical and Experimental Investigation of Helicopter Rotor Hover Performance and Wake Geometry Characteristics,* USAAMRDL Technical Report 71-24, Ft. Eustis, VA, USA, 1971

[13] A.J. Landgrebe, *The Wake Geometry of a Hovering Helicopter Rotor and its Influence on Rotor Performance,* Journal of the American Helicopter Society, Vol. 17, No. 4, USA, 1972

[14] J.D. Kocurek, L.F. Berkowitz, *Velocity Coupling - a new Concept for Hover and Axial Flow Wake Analysis and Design,* AGARD-CP-334, Paper No. 8, 1982

[15] T.A. Egolf, A.J. Landgrebe, *Helicopter Rotor Wake Geometry and Its Influence in Forward Flight. Vol. I - Generalized Wake Geometry and Wake Effect on Rotor Airloads and Performance,* NASA CR 3726, USA, 1983

[16] T.S. Beddoes, *A Wake Model for High Resolution Airloads,* Proceedings of the International Conference on Helicopter Basic Research, Army Research Office, Research Triangle Park, NC, USA, 1985

[17] Y.H. Yu, C. Tung, J.M. Gallman, W.R. Splettstößer, K.J. Schultz, B.G. van der Wall, P. Spiegel, G. Rahier, B. Michéa, M. Costes, *Aerodynamics and Acoustics of Rotor Blade-Vortex Interactions: Analysis Capability and its Validation,* AIAA 93-4332, 15^{th} AIAA Aeroacoustics Conference, Long Beach, CA, USA, 1993

[18] P. Beaumier, J. Prieur, G. Rahier, P. Spiegel, A. Demargne, C. Tung, J.M. Gallman, Y.H. Yu, R. Kube, B.G. van der Wall, K.J. Schultz, W.R. Splettstößer, T.F. Brooks, C.L. Burley, D.D. Boyd, Jr., *Aerodynamic and Acoustic Effects of Higher Harmonic Control on Helicopter Rotor Blade-Vortex Interaction: Predictions and Preliminary Validation,* 75^{th} AGARD Fluid Dynamics Panel Meeting and Symposium on Aerodynamics and Acoustics of Rotorcraft, Berlin, Germany, 1994

[19] R. Kube, B.G. van der Wall, K.J. Schultz, *Mechanisms of Vibration and BVI Noise Reduction by Higher Harmonic Control,* 20^{th} European Rotorcraft Forum, Amsterdam, Netherlands, 1994

[20] Y.H. Yu, C. Tung, J.M. Gallman, K.J. Schultz, B.G. van der Wall, P. Spiegel, B. Michéa, *Aerodynamics and Acoustics of Rotor Blade-Vortex Interactions,* Journal of Aircraft, Vol. 32, No. 5, 1995

[21] C. Tung, J.M. Gallman, R. Kube, W. Wagner, B.G. van der Wall, T.F. Brooks, C.L. Burley, D.D. Boyd, Jr., G. Rahier, P. Beaumier, *Prediction and Measurement of Blade-Vortex Interaction Loading,* 1^{st} Joint CEAS/AIAA Aeroacoustics Conference, Munich, Germany, 1995

[22] P. Beaumier, P. Spiegel, *Validation of ONERA Prediction Methods for Blade-Vortex Interaction using HART Results,* 51^{st} Annual Forum of the American Helicopter Society, Fort Worth, TX, USA, 1995

[23] K. Ehrenfried, W. Geißler, U. Seelhorst, H. Vollmers, *Combined Numerical and Experimental Investigations of BVI-Noise Generation and Radiation from the HART-Test Campaign,* 21^{st} European Rotorcraft Forum, Saint-Petersburg, Russia, 1995

[24] N. Jobard, M. Costes, P. Beaumier, *Three Dimensional BVI Simulation on Aeroelastic Blades Using a New Deforming Grid Approach Coupled to a Free-Wake Analysis,* 52^{nd} Annual Forum of the American Helicopter Society, Washington, DC, USA, 1996

[25] Y.H. Yu, C. Tung, S. Low, *Blade Aeroelastic Effect on Rotor Blade-Vortex Interaction (BVI) Noise,* 52^{nd} Annual Forum of the American Helicopter Society, Washington, DC, USA, 1996

[26] Y.H. Yu, *Rotor Blade-Vortex Interaction Noise: Generating Mechansms and its Control Concepts,* American Helicopter Society Specialist Meeting on Aeromechanics Technology and Product Design for 21^{st} Century, Bridgeport, CT, USA, 1995

[27] R. Kube, W.R. Splettstößer, W. Wagner, U. Seelhorst, Y.H. Yu, C. Tung, P. Beaumier, J. Prieur, G. Rahier, P. Spiegel, A. Boutier, T.F. Brooks, C.L. Burley, D.D. Boyd, Jr., E. Mercker, K. Pengel, *HHC Aeroacoustic*

Rotor Tests in the German Dutch Wind Tunnel: Improving Physical Understanding and Prediction Codes, 52^{nd} Annual Forum of the American Helicopter Society, Washington, DC, USA, 1996

[28] R. Kube, W.R. Splettstößer, W. Wagner, U. Seelhorst, Y.H. Yu, A. Boutier, E. Mercker, *Initial Results from the Higher Harmonic Aeroacoustic Rotor Test (HART) in the German-Dutch Wind Tunnel,* 75^{th} AGARD Fluid Dynamics Panel Meeting and Symposium on Aerodynamics and Acoustics of Rotorcraft, Berlin, Germany, 1994

[29] J.M. Gallman, C. Tung, K.J. Schultz, W.R. Splettstößer, H. Buchholz, P. Spiegel, C.L. Burley, T.F. Brooks, D.D. Boyd, Jr., *Effect of Wake Structure on Blade-Vortex Interaction Phenomena: Acoustic Prediction and Validation,* 1^{st} Joint CEAS/AIAA Aeroacoustics Conference, Munich, Germany, 1995

[30] E. Mercker, K. Pengel, R. Kube, B.G. van der Wall, A. Boutier, F. Micheli, *On the Blade Deformation Measured at a Scaled Helicopter Rotor,* 2^{nd} International Aeromechanics Specialists' Conference, Bridgeport, CT, USA, 1995

[31] Y.H. Yu, B. Gmelin, W.R. Splettstößer, J.J. Philippe, T.F. Brooks, *Helicopter Blade-Vortex Interaction Noise Reduction by Active Rotor Control Technology,* 23^{st} European Rotorcraft Forum, Dresden, Germany, 1997

[32] E. Mercker, *Compilation of Test Data for the HART-Test,* DNW-TR-94.03, DNW Emmeloord, Netherlands, 1994

[33] B.G. van der Wall, *Vortex Characteristics Analysed from HART Data,* 23^{rd} Eropean Rotorcraft Forum, Dresden, Germany, 1997

[34] A. Boutier, J. Lefèvre, F. Micheli, *3D Laser Velocimetry and Blade Tip Attitude Measurements by TART Method within the HART Test Program,* ONERA RTS 5/51432 PY, Chatillon, France, 1996

[35] H. Glauert, *A General theory of the Autogyro,* Aeronautical Research Council Technical Reports and Memoranda No. 1111, England, 1926

[36] J. M. Drees, *A Theory of Airflow Through Rotors and Its Application to Some Helicopter Problems,* Journal of the Helicopter Association of Great Britain, Vol. 3, No. 2, England, 1949

[37] K.W. Mangler, *Calculation of the Induced Velocity Field of a Rotor,* RAE Rep. No. Aero. 2247 (A.R.C. 11562), England, 1948

[38] K.W. Mangler, *Fourier Coefficients for the Downwash at a Helicopter Rotor,* RAE Tech. Note. No. Aero. 1958 (A.R.C. 11694), England, 1948

[39] K.W. Mangler, H.B. Squire, *The Induced Velocity Field of a Rotor,* Aeronautical Research Council Technical Reports and Memoranda No. 2642, England, 1950

[40] I. Bronstein, K. Semendjajew, *Taschenbuch der Mathematik,* 18^{th} Edition, Verlag Harri Deutsch, Thun, Frankfurt/Main, Germany, 1979

[41] S. Wolfram, *Mathematica®*[2], ISBN 3-89319-371-5, Addison-Wesley Publishing GmbH, Germany, 1994

[42] A. Gessow, G.C. Myers, Jr., *Aerodynamics of the helicopter,* ISBN 0-8044-4275-4, College Park Press, MD, USA, 1985

[43] W. Johnson, *Helicopter Theory,* ISBN 0-691-07917-4, Princeton University Press, NJ, USA, 1980

[44] B.G. van der Wall, *Analytic Formulation of Unsteady Aerodynamics and its Application to Simulations of Rotors,* ESA-TT-1244, 1992. Translation of: *Analytische Formulierung der instationären Profilbeiwerte und deren Anwendung in der Rotorsimulation,* DLR-FB 90-28, Braunschweig, Germany, 1990

[45] D. Petot, G. Arnaud, R. Harrison, J. Stevens, D. Teves, B.G. van der Wall, C. Young, E. Szechenyi, *Stall Effects and Blade Torsion - an Evaluation of Predictive Tools,* 23^{rd} European Rotorcraft Forum, Dresden, Germany, 1997

[46] B.G. van der Wall, *Der Einfluß aktiver Blattsteuerung auf die Wirbelbewegung im Nachlauf von Hubschrauberrotoren,* DLR FB 1999-34, Braunschweig, Germany, 1999

[2] Mathematica is a registered trademark of Wolfram Research Inc.